ACS APPLIED MATERIALS & INTERFACES

Research Article

www.acsami.org

Engineering Scaffolds Integrated with Calcium Sulfate and Oyster Shell for Enhanced Bone Tissue Regeneration

Yue Shen,[†,#] Shizhou Yang,[‡,#] Jianli Liu,[∥] Huazi Xu,[§] Zhongli Shi,[†] Zhongqing Lin,[§] Xiaozhou Ying,[§] Peng Guo,[†] Tiao Lin,[†] Shigui Yan,[†,*] Qing Huang,[*,⊥] and Lei Peng[*,∥]

[†]Department of Orthopaedic Surgery, Second Affiliated Hospital, School of Medicine, Zhejiang University, Hangzhou 310009, Zhejiang China

[‡]Department of Gynecologic Oncology, Women's Reproductive Health Key Laboratory of Zhejiang Province, Women's Hospital, School of Medicine, Zhejiang University, Hangzhou 310009, Zhejiang China

[§]Department of Orthopaedic Surgery, Second Affiliated Hospital of Wenzhou Medical University, Wenzhou 325000, Zhejiang China

[∥]Trauma Center of the Affiliated Hospital of Hainan Medical College, Haikou 570206, Hainan China

[⊥]Division of Functional Materials and Nanodevices, Ningbo Institute of Materials Technology and Engineering (NIMTE), Chinese Academy of Sciences (CAS), Ningbo 315201, Zhejiang China

Supporting Information

ABSTRACT: Engineering scaffolds combinging natural biomineral and artificially synthesized material hold promising potential for bone tissue regeneration. In this study, novel bioactive calcium sulfate/oyster shell (CS/OS) composites were prepared. Comparing to CS scaffold, the CS/OS composites with a controllable degradation rate displayed enhanced mineral nodule formation, higher alkaline phosphate (ALP) activity and increased proliferation rate while treated osteocytes. In CS/OS composites group, elevated mRNA levels of key osteogenic genes including bone morphogenetic protein-2 (BMP-2), runt-related transcription factor 2 (Runx2), osterix (Osx), and osteocalcin (OCN) were observed. Furthermore, The up-regulation of BMP-2 and type I collagen (COL-I) was observed for CS/OS composites relative to a CS group. Scaffolds were implanted into critical-sized femur cavity defects in rabbits to investigate the osteogenic capacity of the composites in vivo. The CS/OS scaffolds with proper suitable times and mechanical strength strongly promoted osteogenic tissue regeneration relative to the regeneration capacity of CS scaffolds, as indicated by the results of histological staining. These results suggest that the OS-modified CS engineering scaffolds with improved mechanical properties and bioactivity would facilitate the development of a new strategy for clinic bone defect regeneration.

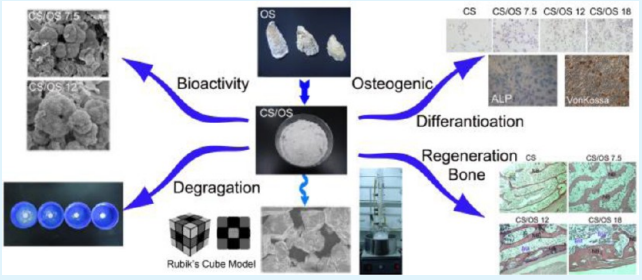

KEYWORDS: *calcium sulfate, oyster shell, bioactivity, osteogenic differentiation, femur defect, osteogenesis*

1. INTRODUCTION

Bone defects and nonunion are the problems most frequently encountered in modern reconstructive orthopedic surgery. Autografting and allografting are the "gold standard" for treating these diseases. However, these bone grafting techniques cannot be applied widely due to their intrinsic drawbacks.[1] For example, autografting and allografting are severely restricted by the scarce supply of donors. Moreover, great concerns exist regarding the pain and complications such as infection and hematoma caused by donor harvesting[2,3] and immune response.[4] In addition, the grafting techniques require critical defect sizes and host−bed viability.[5,6] Therefore, several factitial bone substitutes with excellent biocompatibility have been developed as implantable grafts. Strict requirements are set for ideal factitial bone substitutes.[1] For example, substitutes should exhibit excellent biocompatibility and suitable mechanical strength to serve as scaffolds for new bone growth and should be osteoinductive and osteoconductive to accelerate bone formation. Finally, substitutes should be biodegradable when completely replaced by new bone tissue. Single biomaterials can hardly fulfill all of the above-mentioned requirements. Therefore, synthesized composites are attracting widespread attention for use as bone grafts.

Calcium sulfate hemihydrate ($CaSO_4 \cdot {}^1/_2H_2O$, CSH) has a clinical application history spanning over 100 years due to its excellent biocompatibility and osteoconductivity. The transformation of CSH into calcium sulfate dihydrate ($CaSO_4 \cdot 2H_2O$, CSD) by reacting with water has been exploited to produce calcium sulfate ($CaSO_4$, CS) cement for bone augmentation,[7] drug carriers[8,9] and bone graft substitutes.[7]

Received: March 11, 2014
Accepted: July 17, 2014
Published: July 17, 2014

However, the resorption rate of the calcium sulfate cement is too fast to match the rate of new bone formation, which creates negative effects on bone regeneration.[10,11] Furthermore, neither the pH environment nor the ion release behavior of calcium sulfate is suitable for bone regeneration because it fails to provide an appropriate microenvironment for bone defects.[11,12] Recently, calcium sulfate composites have been widely studied to overcome the above-mentioned clinical challenges. Cabanas et al.[10] introduced hydroxyapatite into calcium sulfate to form composite cements. Lei et al.[13] reported a suitable composite filler consisting of 60% $CaSO_4$ and 40% HA by mass. Mamidwar and Cao[14−16] described a $CaSO_4$/PLLA composite that presents a delayed degradation rate. However, no study has attempted to modify $CaSO_4$ by combining it with a natural biomineral. Recent studies have opened new avenues of research by investigating natural biominerals as bone grafts. Oyster shell (OS), mainly composed of calcium carbonate biomineral, is considered a suitable bone substitute.[17] In 2004, an article in *Science* reported that the biomineralization process of oyster shell is similar to osteogenesis in the human body.[18]

Bone tissue consists of mineral and an organic matrix, such as hydroxyapatite and bone cells. Type I collagen (COL-I) secreted by osteoblasts can serve as a scaffold during the physiological process of new bone tissue formation (90%), with the remaining material (10%) composed of noncollagenous proteins include osteonectin, osteocalcin (OCN), and osteopontin.[19] In addition, osteoblasts also secrete growth factors to induce immobilization in bone matrix. Runt-related transcription factor 2 (Runx2) is an indispensable transcription factor for osteoblast differentiation both during endochondral and intramembranous ossification.[20] Bone morphogenetic protein-2 (BMP-2), which plays a prominent role in fracture healing, is essential for maintaining bone homeostasis. BMP-2 is also known to regulate osteogenic transcription factors such as Runx-2 and Osterix.[21] Osterix, a zinc finger-containing transcription factor, regulates gene expression in committed osteoblastic precursor cells to promote differentiation.[20] Many studies[22−26] have demonstrated that nacre exhibits satisfactory biocompatibility, osteoinduction, and slow resorption rates in vivo. Shen et al.[26] showed that nacre contains various signaling molecules that can activate the osteogenic differentiation of bone marrow cells. Mouries et al.[27] proved their initial hypothesis that nacre organic matrix (WSM) contains signaling molecules that can stimulate the osteogenic pathway in mammalian cells. Therefore, it is reasonable to incorporate oyster shell into calcium sulfate to produce composite cements with improved properties, and the composite can be expected to be a natural carrier of bone growth factors to enhance osteogenetic processes.

In the present study, calcium sulfate/oyster shell (CS/OS) composites were produced through a salt solution method. The setting behavior, mechanical properties, and in vitro degradability of the composites were studied in detail. The bioactivity of the composites was evaluated to assess the composites' safety and potential in promoting osteogenesis. Then, the cellular response for osteogenic differentiation was investigated at the level of mRNA expression and protein changes. An in vivo rabbit femur cavity defect model was used to evaluate the bone tissue regeneration ability of the CS/OS composites.

2. MATERIALS AND METHODS

2.1. Preparation and Characterization of CS/OS Composites. All starting chemicals were of analytical grade and purchased from Sinopharm Chemical Reagent Co. Ltd. (Shanghai, China). Succinic acid and 99.7 wt % absolute ethanol were used as the morphology-modifying agents. A $CaCl_2$ solution was used as the medium for the conversion from CSD to α-CSH. The oyster shells were derived from Zhejiang Wenzhou offshore oysters. After flushed under water flow to remove sand particles, the oyster shells were immersed in 40% acetic acid for 60 min to eliminate the organic components on the surface. The treated oyster shells were then flushed and immersed in distilled water for 6 h until they reached neutral pH. Then, the oyster shells were crushed and ball milled for 6 h to obtain fine powders. The powders were successively soaked in a mixture of chloroform and methanol at a volume ratio of 1:1 for 24 h. Then, the powders were flushed and immersed in distilled water for 6 h. The powders were subsequently soaked in 30% hydrogen peroxide for 48 h to eliminate the antigen. Finally, the treated powders were flushed and dried and then sieved through a 100-mesh filter to yield fine oyster shell powders.

A salt solution method was used to prepare the calcium sulfate/oyster shell (CS/OS) composites based on our previous work.[28] The reaction was carried out in a three-neck flask equipped with a reflux condenser for vapor reflux. The reaction temperature was maintained at 110 °C using an oil bath. In a typical synthesis, a 30 wt % $CaCl_2$ aqueous solution containing a 2:3 ethanol/water solution and 0.25 wt % succinic acid (to CSD powders) was prepared as the reaction medium. The solution was stirred homogeneously using a magnetic stirrer for 30 min. After that, the prepared solution was transferred into the three-neck flask keeping in an oil bath and preheated to 110 °C with magnetic stirring. CSD powders and the obtained oyster shell powders were subsequently added into the flask and reacted for 48 h. Finally, the resulting powders were rapidly filtered and dried at 110 °C for 30 min in an oven. CS/OS composites with different OS contents of 0, 7.5, 12, and 18 wt % were prepared and labeled as CS, CS/OS7.5, CS/OS12/ and CS/OS18, respectively. The obtained CS/OS composites were examined using X-ray diffraction (XRD, Bruker D8 Advance, Germany) with Cu radiation at a scanning rate of 15°/min over the 2θ range from 10° to 90°. The morphologies of the composites were investigated using a field emission scanning electron microscope (FE-SEM, S-4800, Japan).

2.2. Characterization of Setting and Mechanical Properties. Pastes of CS, CS/OS7.5, CS/OS12, and CS/OS18 were formed by mixing the obtained composite powders with distilled water in a liquid/powder (L/P) weight ratio of 0.7 mL g^{-1}. The setting properties of the pastes were measured using a Vicat needle according to ISO9597-1989E. The initial setting time is defined as the time necessary for the light needle (280 g, Φ 1.13 mm) to plunge into a paste and leave a span of 5 ± 1 mm to the tube bottom. The final setting time is defined as the time necessary for the heavy needle (350 g, Φ 2.0 mm) to no longer leave a visible print on the surface of a paste. Each test was repeated six times, and a statistical method was used to analyze the results.

The CS, CS/OS7.5, CS/OS12, CS/OS18, and CS/OS25 pastes were placed in separate Teflon molds (Φ 6 mm × 12 mm) to form cylindrical specimens. After the specimens solidified, they were removed from the molds. To obtain suitable mechanical properties, the specimens were incubated at 37 °C with 100% relative humidity for various incubation times of 1, 7, 14, 21, and 28 days. The compressive strengths of the specimens were tested using an Instron (Instron 5800, America) at a loading rate of 0.5 mm/min.

2.3. In Vitro Bioactivity. The in vitro bioactivity of the CS/OS composites was evaluated using the simulated body fluid method. Simulated body fluid (SBF) was prepared according to the procedure described by Kokubo.[29] The CS, CS/OS7.5, CS/OS12, and CS/OS18 pastes were placed in Teflon molds (Φ 6 mm × 3 mm) to form disk-shaped specimens. The specimens were pretreated by incubating at 37 °C with 100% relative humidity for 14 days. They were then separately immersed in the SBF solution with a surface area/volume ratio[30] of 0.1 cm^{-1} and maintained at 37 °C in a shaking water bath for 7 days. The SBF solution was refreshed every day. Then, the disks were gently rinsed with deionized water and dried at room temperature. The

specimens were examined using XRD and a FE-SEM with an energy-dispersive X-ray detector (EDX, FE-SEM, S-4800, Japan).

2.4. In Vitro Degradation Test. Groups of CS, CS/OS7.5, CS/OS12, and CS/OS18 specimens (Φ 6 mm × 3 mm) were soaked in SBF solutions for 4, 7, 10, 14, 21, and 28 days in a shaking water bath. The SBF solutions were refreshed every 2 days. After each soaking period, the specimens were removed from solution and dried at 60 °C for 12 h. The weights of the specimens were measured before and after testing to determine the weight loss. The other group of CS, CS/OS7.5, CS/OS12, and CS/OS18 specimens (Φ 6 mm × 3 mm) was separately immersed in the SBF solution without refreshing, and the soaking solutions were collected each soaking period. The Ca^{2+} concentrations and pH values of the soaking solutions were examined using inductively coupled plasma–atomic emission spectrometry (ICP-AES, Optima 2100, U.S.A.) and an electrolyte-type pH meter (FE20K, Mettler Toledo, Switzerland).

2.5. Cell Culture. MG-63, a human osteosarcoma cell line with osteoblastic potential, purchased from the Cell Culture Center, Chinese Academy of Medical Science (CCC, CAMS, China), was selected for evaluation. MG-63 cells were seeded in Dulbecco's Modified Eagle Medium (DMEM, Gibco, U.S.A.) supplemented with 10% (V/V) fetal bovine serum (FBS, Gibco, U.S.A.) at 37 °C in a humidified atmosphere with 5% CO_2, then detached with 0.25% trypsin/0.03% ethylene diamine tetraacetic acid (EDTA). The cell density was calculated, allowing for the desired density to be used in later experiments. After 24 h, the cells were treated with 50 mg/mL concentrations of dissolution extracts from the above-described CS, CS/OS7.5, CS/OS12, and CS/OS18 specimens. The cell groups of the related tests were as follows: CS, CS/OS7.5, CS/OS12, and CS/OS18.

2.5.1. Cell Viability. The 7-day-preincubated CS, CS/OS7.5, CS/OS12, and CS/OS18 specimens were crushed into 300-mesh fine powders for cytotoxicity testing. Dissolution extracts were prepared by adding powders to DMEM cell culture medium for 1 day at 37 °C in a humidified atmosphere of 5% CO_2, with medium concentrations of 6.25, 12.5, 25, 50, 100, and 200 mg/mL. After incubation, the mixture was centrifuged, and the supernatant was collected. For cell proliferation assays, a 100-μL MG-63 cell suspension with a density of 1×10^4 cells/mL was added to each well of a 96-well plate and incubated for 24 h. The culture medium was removed and replaced by 100 μL extracts. DMEM (10% FBS) without added extracts was used as a control. After incubating at 37 °C and 5% CO_2 for 1, 4, and 7 days, the Cell Counting Kit-8 (CCK-8, Dojindo, Japan) was used to determine the proliferation of MG63 according to the manufacturer's instructions. Briefly, CCK-8 solution was added to 96-well plates, then the cells were incubated for 120 min, and absorbance was measured at 570 nm using an MRX Revelation 96-well multiscanner (Dynex Technologies, Chantilly, VA). This experiment was repeated six times.

2.5.2. Determination of Alkaline Phosphatase (ALP) Activity. Cells were inoculated at 1×10^4/mL in 24-well plates. Alkaline phosphate (ALP) staining was performed at the seventh day. Cells were rinsed twice with phosphate-buffered saline (PBS) and then fixed with 4% paraformaldehyde. An ALP substrate mixture was then added and incubated for 10 min. The ALP activity was quantified at a wavelength of 405 nm using a microplate reader (SPECTRAmax 384, Molecular Devices) as the substrate, and the total protein contents in the cell lysate were determined using the bicinchoninic acid method in aliquots of the same samples with a Pierce protein assay kit (Pierce Biotechnology Inc., Rockford, IL, U.S.A.), read at 562 nm and calculated according to a series of albumin (bovine serum albumin) standards. The ALP levels were normalized to the total protein content and performed in quadruplicate for all of the experiments.

2.5.3. Quantitation of Mineralized Nodule Formation. To qualitatively assess cell-mediated calcium deposition, MG-63 cells were visualized by Von Kossa staining. After 24 h of culturing in 24-well tissue culture plates at a cell density of 1×10^4, cells were treated with the same concentrations of dissolution extracts described above. Von Kossa staining was performed at the 18th day. Cells in the well plates were fixed in 4% paraformaldehyde, stained with 1% silver nitrate, placed under a UV lamp for 30 min and rinsed with distilled water before treatment with 5% sodium thiosulfate for 2 min. Von Kossa-positive deposits were observed after washing with alcohol. Calcium mineralized nodules with a diameter greater than 1 mm were counted and analyzed.

2.5.4. Real-Time Polymerase Chain Reaction (PCR) Analysis. Real-time PCR was used to detect the expression of several osteogenic differentiation-related marker genes (BMP-2, Runx2, Osterix, and OCN) at the 4th, 7th, and 14th days. Total RNA was extracted using TriZol (Invitrogen) according to the manufacturer's instructions. Its concentration was determined by NanoDrop 2000c (Thermo Fisher Scientific Inc. U.S.A.). First strand complementary DNAs (cDNAs) were synthesized from 1 μg of the isolated RNA by oligo-(deoxythymidine) (oligo(dT)) using DyNamoTM cDNA Synthesis Kit (Fermentas), and used as templates for real-time PCR. The PCR was performed on a final volume of 25 μL containing 3 μL cDNA, 2 μL of each primer, 1 μL ROX reference dye, and 12.5 μL of SYBR Green Master mix (TIANGEN), with ABI Prism 7300 (Applied Biosystems, Foster City, CA, U.S.A.). The expression of mRNAs was determined quantitatively using DyNamo SYBR1 Green qPCR kit (Takara, Japan). The primers were as follows: for BMP-2, sense primer, 5′-ACC CGC TGT CTT CTA GCG T-3′, and antisense primer, 5′-TTT CAG GCC GAA CAT GCT GAG-3′; for Runx2, sense primer, 5′-CCC CAC GAC AAC CGC ACC AT-3′, and antisense primer, 5′-CAC TCC GGC CCA CAA ATC-3′; for Osterix, sense primer, 5′-CTC CTG CGA CTG CCC TAA T-3′ and antisense primer, 5′-ATA CTT CTG GGT CTT GGG CAT-3′; for OCN, sense primer, 5′-GGC CAG GCA GGT GCG AAG C-3′, and antisense primer, 5′-GCC AGG CCA GCA GAG CGA CAC-3′; for GAPDH, sense primer, 5′-GAA GTG GAA GGT CGG AGT C-3′, antisense primer, 5′-GAA GAT GGT GAT GGG ATT TC-3′. The samples underwent 40 cycles consisting of the following steps: initial denaturation at 95 °C for 10 min, followed by a set cycle of denaturation at 95 °C for 15 s, different annealing temperatures for each pair of primers (ranging between 53 and 68 °C) for 15 s, extension at 72 °C for 32 s and a final elongation at 72 °C for 5 min. Fold increment of any assayed gene was calculated by normalizing its expression level to that of the glyceraldehyde-3-phosphate dehydrogenase (GAPDH) gene, which was used as an internal control.

2.5.5. Immunochemical Staining and Western Blot Analysis. Expression of BMP-2 in MG-63 cells was examined by immunochemical staining. Briefly, endogenous peroxidase activity was blocked by incubation with 3% hydrogen peroxide for 45 min. Nonspecific binding was blocked by incubation in goat serum albumin. The section was then incubated at 4 °C for 12 h with mouse antihuman BMP-2 monoclonal antibody (Santa Cruz, CA) diluted in PBS (1:200), followed by incubation with 1:100 diluted horseradish peroxidase (HRP)-conjugated rabbit antimouse antibody (DAKO, Carpinteria, CA) for 30 min. Color was developed with diaminobenzidine tetrahydrochloride (DAB).

After incubation, at the seventh and 12th days, cells were washed with ice-cold PBS and lysed in NP 40 lysis buffer. Cells without composite extracts treatment were defined as control group. Protein was extracted using Mammalian Protein Extraction Reagent (Pierce Inc., Rockford, IL) and its concentration was determined by BCA (Pierce, Rockford, IL, U.S.A.) assay. Proteins (30 μg) were separated in 12% SDS-PAGE and transferred to PVDF membrane. Membranes were incubated with primary antibody overnight at 4 °C, and then with the respective secondary antibodies. Immunoreactive bands were detected by the enhanced chemiluminescence (ECL) kit for Western blotting detection with hyper-ECL film. The same membrane was reprobed with the anti-GAPDH antibody, which was used as an internal control for protein loading.

2.6. Femur Cavity Defect Repair. An orthotopic study using a rabbit femur cavity defect model was carried out to investigate the efficacy of the CS/OS composites in promoting bone repair and regeneration. Twenty-four female New Zealand rabbits (mean body weight 2.5 kg) were divided into four groups (CS, CS/OS7.5, CS/OS12, and CS/OS18). The rabbits were anesthetized by intramuscular injection of sodium pentobarbital (0.02 g/kg, Sigma) and operated on under rigorous aseptic conditions. Then, a critical-sized (8 mm-

diameter, Φ 8 × 5 mm) circular defect oriented perpendicular to the longitudinal and sagittal axes of the femur was made in each animal. The CS, CS/OS7.5, CS/OS12, and CS/OS18 composites were then implanted into the cavities. After 8 weeks, the rabbits were sacrificed and specimens were harvested. Histological evaluation was performed. The extracted femora, with soft tissue cleaned, were fixed in neutral buffered formalin, decalcified in formic acid, embedded in paraffin, sectioned (5 μm thick) and then deparaffinized with xylene, followed by hydration in ethanol solutions of decreasing concentration (100–70%). Bone regeneration histology was observed by hematoxylin and eosin (H&E) staining. The experimental protocol was approved by the Institutional Animal Care and Use Committee of the Laboratory Animal Center of Zhejiang University.

2.7. Statistical Analysis. All numerical data are expressed as means ± standard deviations. Statistical analysis was performed by one-way analysis of variance (ANOVA). A value of $p < 0.05$ was considered indicative of statistical significance.

3. RESULTS

3.1. Composite Preparation and Characterization. Figure 1a shows the XRD patterns of the pure CS and CS/OS composites as well as that of natural OS powder. In the spectrum of the CS/OS composite powder, all peaks are related to the calcium sulfate hemihydrate phase (JCPDS card 74-1433) with a monoclinic structure and the calcium carbonate phase (JCPDS card 85-1108). The obtained CSH phase is in good agreement with previously reported results.[31] No additional phase was observed, indicating that the existence of OS particles had no effect on the crystallization of the calcium sulfate hemihydrate phase. Calcium carbonate with the Rhombo.H.axes structure was identified as the main component of natural OS.

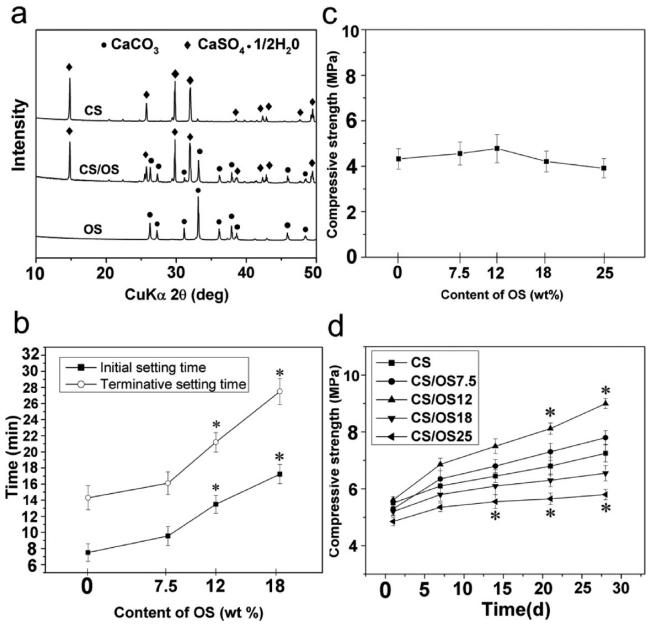

Figure 1. (a) XRD patterns of samples before self-setting process: pure CSH, CS/OS composite cement powder and OS powder. (b) Initial and terminative setting time for the CS/OS composite cements. (c) The compressive strength of the composite cement after final setting. (d) The compressive strength of the CS/OS with different ratio of OS after setting for various incubating time. * Statistically significant difference between the composite pastes and pure CS cement (*$p < 0.05$, Student's t test).

Figure 2 shows SEM micrographs of the resulting powders, including the pure CSH, the CS/OS composite, and the original OS. The pure CSH powders consisted of well-crystallized hexagonal prism grains with a length of 30 μm (length/width ratio of 1:1). Fine particles measuring 2–10 μm and large aggregates could be observed in the OS powders. In the CS/OS composite powders, it was observed that the OS particles tended to aggregate around the CSH grains and surround them, which would alter the surface characteristics of the CSH grains.

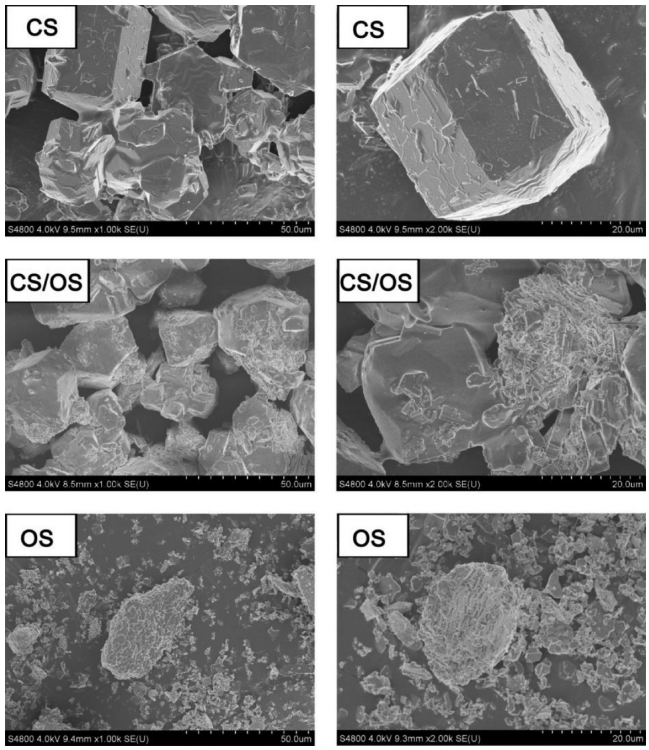

Figure 2. SEM images of the calcium sulfate hemihydrates powder (CS), calcium Sulfate hemihydrate/oyster shell composite cement powder (CS/OS) and oyster shell powder (OS).

3.2. Setting Time and Mechanical Strength of the Composites. Figure 1b shows the initial and terminative setting times of the CS, CS/OS7.5, CS/OS12, and CS/OS18 composites. It was observed that the setting time increased with the addition of OS. The CS/OS18 composite showed the longest initial setting time of 18 min and terminative setting time of 28 min. This finding indicates that the OS additive had a retarding effect on the setting time of the composites. Figure S1 of the Supporting Information presents the surface morphology of the specimens before soaking in SBF. The self-setting process of CSH leading to the formation of CSD crystals can explain the remodeling process of the composites' morphological structure. Figure 1 (c and d) shows the compressive strengths of the CS, CS/OS7.5, CS/OS12, CS/OS18, and CS/OS25 specimens. The results indicate that the compressive strengths of the specimens ranged from 3.9 to 4.7 MPa, with no significant differences observed between composite samples (Figure 1c). Furthermore, Figure 1d shows that the compressive strengths of the CS/OS after incubation increased when the amount of OS added was below 12 wt %. In contrast, after incubation, the compressive strengths decreased sharply as the OS content surpassed 12

wt %. The compressive strength of the CS/OS12 composite was the highest whereas that of the CS/OS25 composite was lowest among all samples observed ($p < 0.05$). Due to its poor mechanical performance, we excluded the CS/OS25 group from following experiments.

3.3. Bioactivity In Vitro. Figure 3 shows the surface morphology of specimens with different OS contents after soaking in SBF solution for 7 days. The surface morphology of CS/OS18 after soaking is shown in Supporting Information Figure S2. Compared to the pure CS specimen, the CS/OS7.5, CS/OS12, and CS/OS18 specimens exhibited new apatite layers on the surface of grains. The apatite layers consisted of clusters of tiny crystals measuring 20−40 nm. The EDX pattern shown in Figure 4a further demonstrates that the apatite layer was mainly composed of calcium and phosphorus. The powders of the soaked specimens were analyzed by XRD, the results of which are shown in Figure 4b. Only calcium sulfate dehydrate (CSD) and CSH were detected in the pure CS specimen group after SBF soaking. However, in the soaked CS/OS composite specimens, the main diffraction peaks for CSD/CSH and calcium carbonate and the characteristic diffraction peaks for bone-like apatite appeared in the spectrum of the CS/OS12 group.

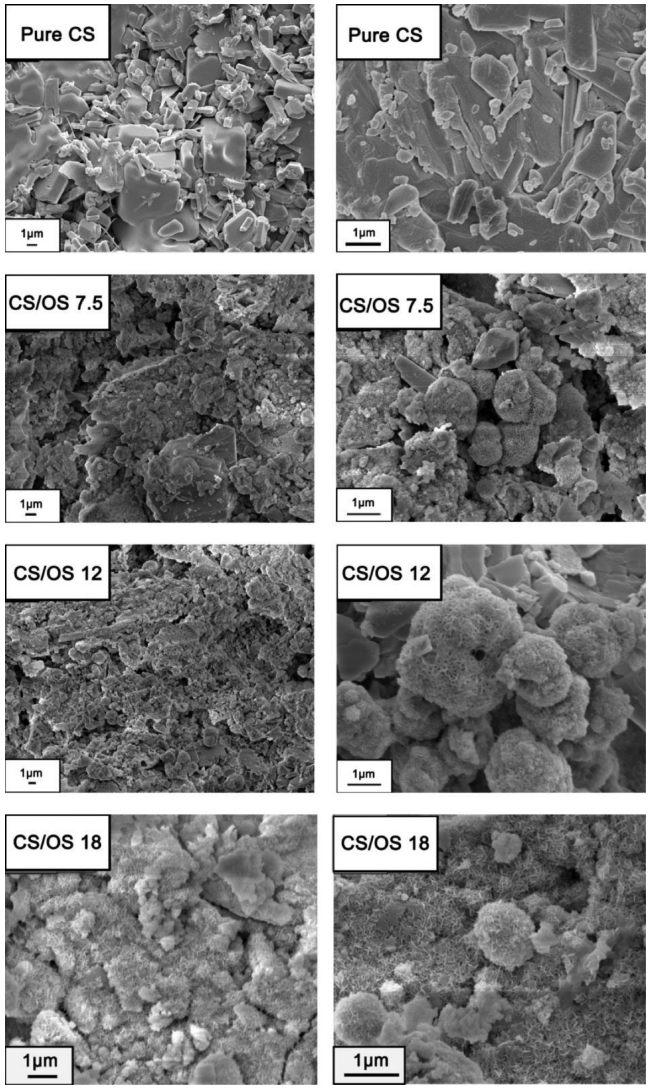

Figure 3. SEM images on the surface of the pure CS cement (CS) and calcium sulfate/oyster shell composite cement with 7.5 wt % OS (CS/OS7.5), composite cement with 12 wt % OS (CS/OS12), and composite cement with 18 wt % OS (CS/OS18) after soaking in SBF for 7 days.

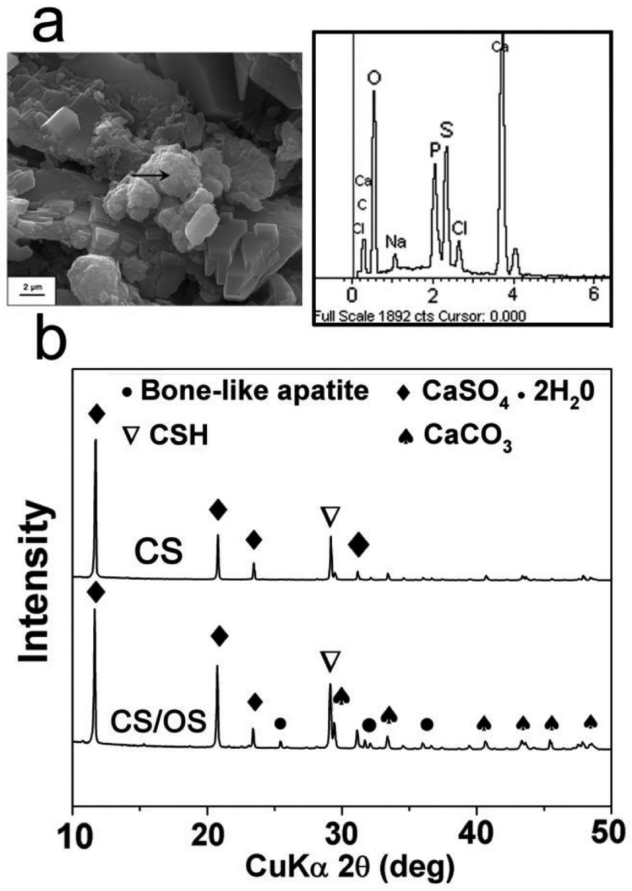

Figure 4. (a) EDX analysis of the arrowed precipitate on the surface of the CS/OS12 composite after soaking in SBF for 7 days showing the presence of elements of Ca, P, O, and C. (b) XRD patterns of the Pure CS and CS/OS12 composite after soaking in SBF for 7 days.

3.4. Ca^{2+} Release and pH in SBF. Figure 5 shows the changes in the calcium ion concentration and pH values of the SBF solution after SBF soaking. It is worth noting that the pure CS specimens released more Ca^{2+} than did the CS/OS composites at the same instant in time (Figure 5a). All samples containing pure CS and CS/OS composites showed an alkaline to acidic pH transition (Figure 5b). However, the addition of OS powder effectively alleviated the process of acidification.

3.5. Degradation In Vitro. Figure 5c shows the degradation rate of the composite specimens after soaking in SBF solution. It can be clearly observed that the pure CS specimens degraded rapidly in SBF solution. However, with the addition of OS, the degradation of the composite specimens was significantly delayed relative to that of the pure CS. In addition, the rate of degradation decreased with increasing OS content in the composites. The CS/OS18 composite specimens showed the lowest degradation rate among all observed samples after 28 days soaking.

3.6. Cell Proliferation. Figure 6 shows that the extracts of the pure CS and CS/OS composite pastes showed no significant cytotoxicity against MG-63 cells after incubation for 1, 4, and 7 days. This result indicates that OS addition

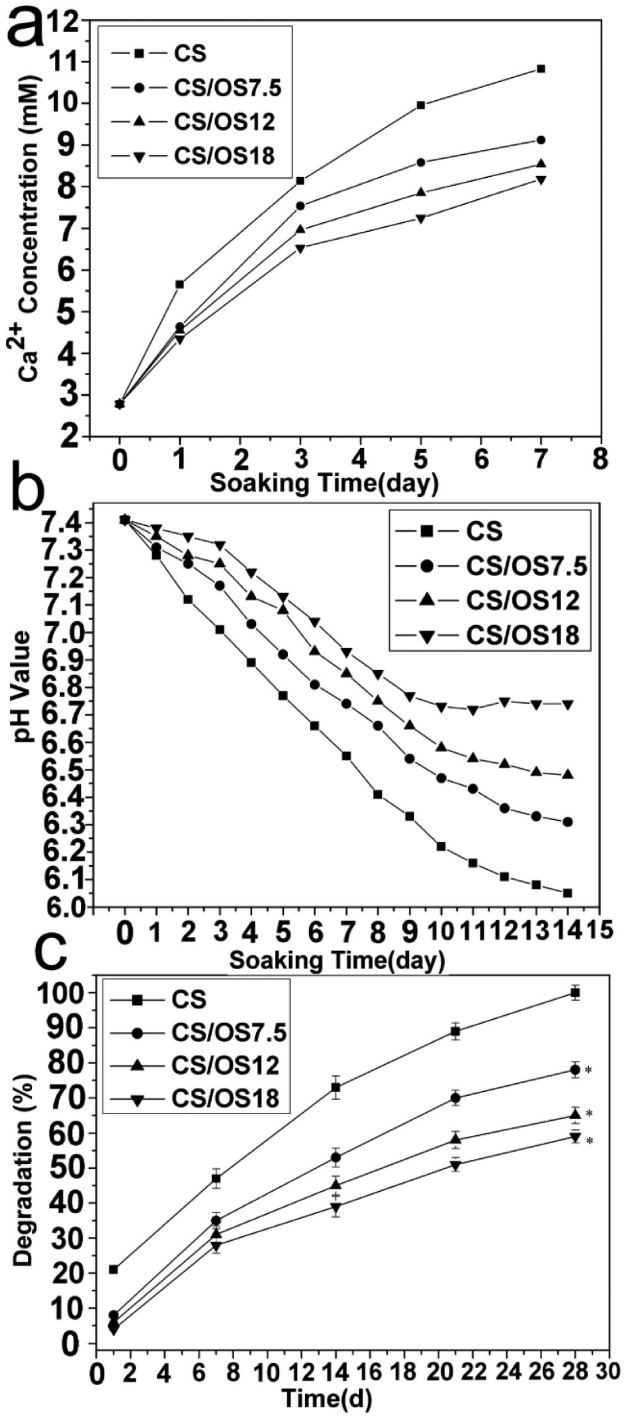

Figure 5. Dependent of Ca concentration (a) and the pH value (b) in the SBF solution of CS/OS composite cements during soaking time. (c) Degradation of CS/OS composite cements after soaking in SBF. * Statistically significant difference between the degradation rates of CS/OS and pure CS cement (*p < 0.05, Student's t test).

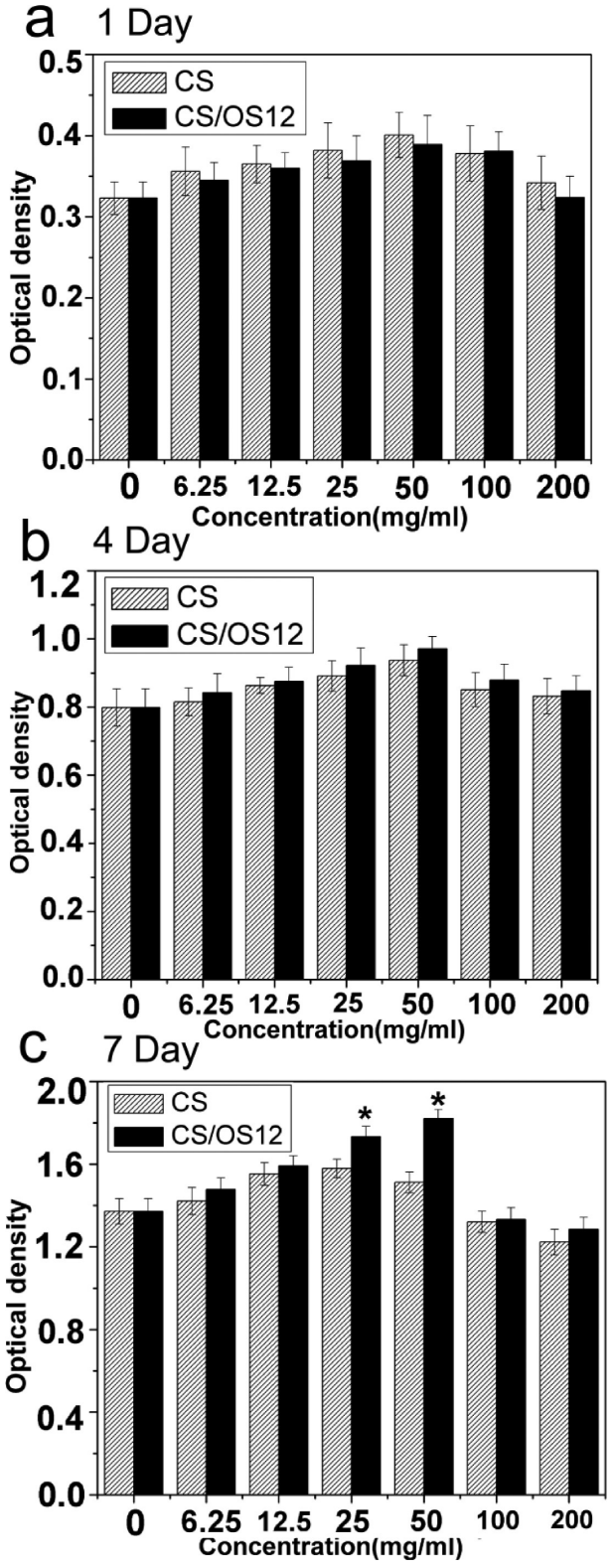

Figure 6. Cell proliferation in the presence of the dissolution extracts of the cement after culturing for different periods. (a) 1 day; (b) 4 day; (c) 7 day. * Significant difference between the CS/OS12 composite and pure CS cement, *p < 0.05.

caused no adverse effect; indeed, the biocompatibility of CS cement has been well documented in previous studies.[31] Furthermore, after incubating for 7 days, the MG-63 cell proliferation of the CS/OS composite was significantly higher than that of the negative control (p < 0.05) at concentrations ranging from 25 to 50 mg/mL. In Supporting Information Figure S3 and S4, the cell proliferation assays of the CS/OS7.5 and 18 composite pastes present a trend similar to that of CS/OS12.

3.7. ALP and Von Kossa Staining. Figure 7a shows the results of ALP staining performed at the seventh day. As shown

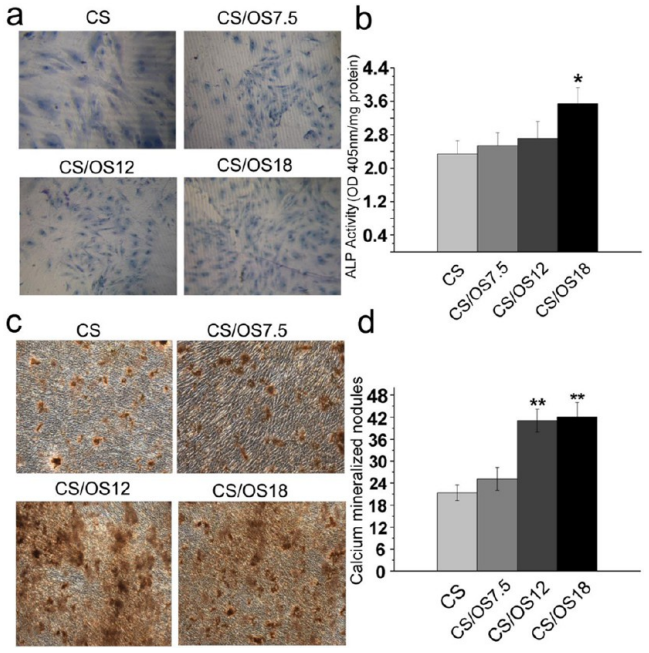

Figure 7. Alkaline phosphatas (ALP) staining (a) was performed at 7th day and quantified (b) after treated with dissolution extracts from CS, CS/OS7.5, CS/OS12, and CS/OS18. Von Kossa staining (c) was applied at 18th day and quantified (d) after dissolution treatment. * Significant difference between the CS/OS composite pastes and pure CS cement, *$p < 0.05$, ** $p < 0.01$.

in Figure 7b, MG-63 cells treated with dissolution extracts from CS/OS18 presented a higher ALP activity than that exhibited by the CS group ($p < 0.05$). The degree of matrix mineralization (calcium precipitation) was also measured by Von Kossa staining at the 18th day (Figure 7c). Figure 7d shows that there were no significant changes in calcium deposition between the CS/OS7.5 group and CS group ($p > 0.05$). However, the extent of calcium deposition was greater in the CS/OS12 and CS/OS18 groups ($p < 0.01$). Thus, it is clear that both the deposition of calcium nodules and ALP activity were enhanced in the CS/OS composite groups.

3.8. The mRNA Expression by Real-time PCR. Real-time PCR (Figure 8) was carried out to detect gene expression during osteogenic differentiation. MG-63 cells treated by dissolution (CS/OS12 and 18) exhibited higher gene expression of BMP-2 and Runx2 at the seventh day than cells treated with pure CS (Figure 8a and b). Compared with that observed for the CS group, the expression of Osterix and OCN was significantly increased when MG-63 cells were cultured with the dissolution of the CS/OS composites (12 and 18%) at the 7th and 14th days (Figure 8c and d).

3.9. Immunochemical Staining and Western Blot Analysis. Immunochemical staining (Figure 9a) revealed that the CS/OS composite groups presented more BMP-2 positive cells as the OS content increased. The expression of osteogenic markers (BMP-2 and COL-I) was also investigated at the protein level by Western blot analysis. At the seventh day, it showed that BMP-2 and COL-I protein were strongly

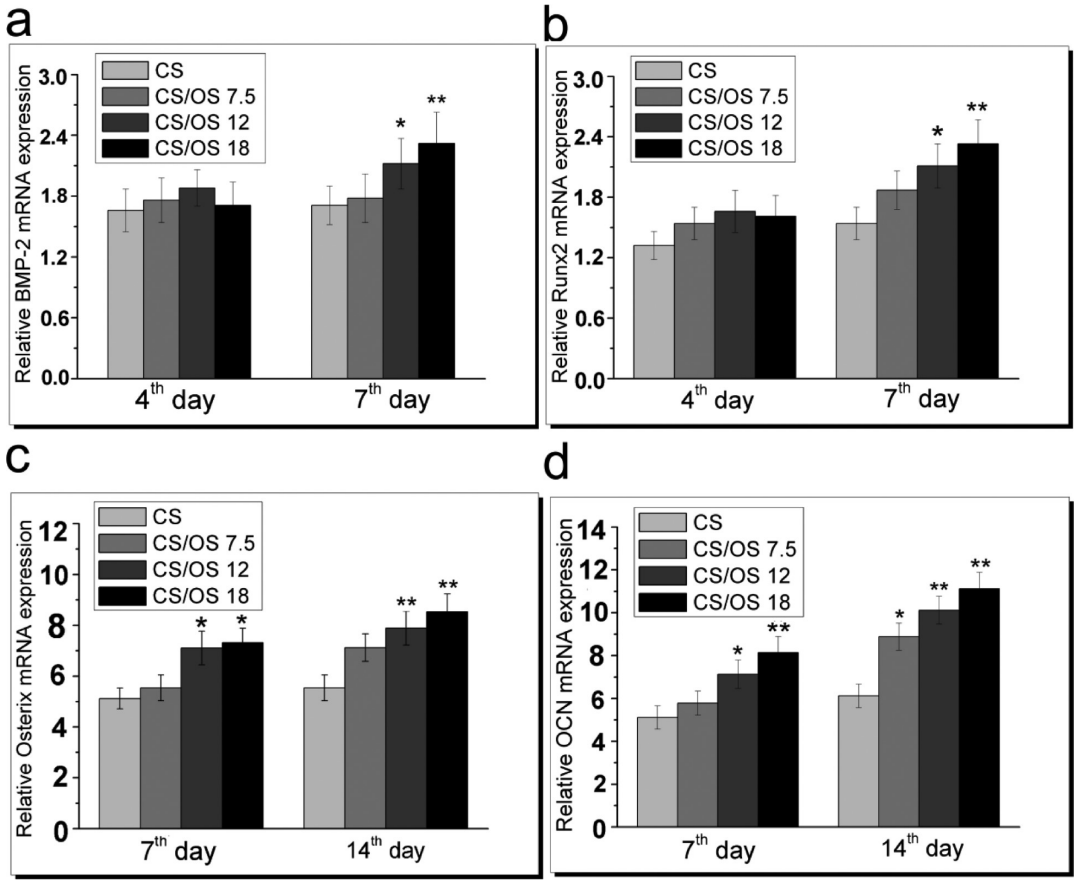

Figure 8. MRNA expression by Real-time PCR (a BMP-2; b Runx2; c Osterix; d OCN) * Significant difference between the CS/OS composite pastes and pure CS cement, *$p < 0.05$, ** $p < 0.01$.

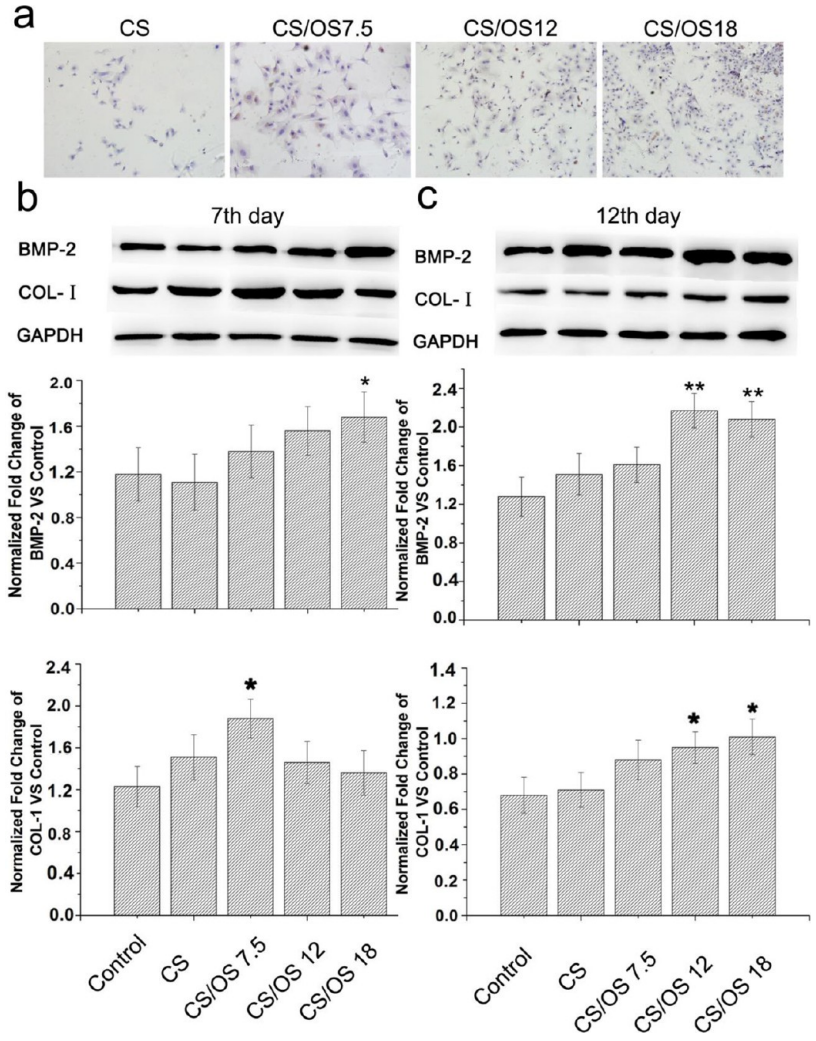

Figure 9. Immunochemical staining (a) and Western Blot analysis at the 7th day (b) and the 12th day (c). * Significant difference between the CS/OS composite pastes and pure CS cement, *$p < 0.05$, ** $p < 0.01$.

expressed in CS/OS composite groups (Figure 9b). Furthermore, CS/OS18 and CS/OS7.5 showed the highest protein level of BMP-2 and COL-I ($P < 0.05$). At the 12th day (Figure 9c), the levels of both BMP-2 and COL-I increased in the CS/OS composite group, with the CS/OS18 composite exhibiting a greater amount of osteogenic markers than the CS group.

3.10. Histological Staining with H&E in Rabbit Femoral Defects. Different CS/OS composite specimens were implanted in rabbit femoral defects, and H&E staining was carried out to evaluate the capability for new bone formation. Histological evidence further supported the in vitro findings, indicating that the specimens of the CS/OS composites showed nearly complete osseous repair of defects, with a typical organized mature bone morphology and noticeable marrow spaces (Figure 10a). In contrast, histological analysis indicated a small amount of irregularly arranged bone tissue and reduced bone formation in the CS group. The percentage of new bone area after 8 weeks was 30.45 ± 4.92% in the CS/OS18 group, 28.6 ± 4.72% in the CS/OS12 group, 20.5 ± 4.12% in the CS/OS7.5 group, and 18.4 ± 3.51% in the CS group (Figure 10b).

4. DISCUSSION

Bone mineral is an important component of the skeleton for support and movement as well as maintaining calcium homeostasis in the body.[31] Calcium sulfate is widely used as a bone cement due to its superior biocompatibility and complete resorption ability. However, calcium sulfate's excessively fast resorption rate and low mechanical strength have limited its applications. In this study, oyster shell (OS) powder, composed of natural $CaCO_3$ minerals, was introduced into calcium sulfate. The resulting composite was expected to combine the self-setting ability of calcium sulfate and the bioactivity of oyster shells.[22,23,32,33]

4.1. Self-Setting Properties of the CS/OS Composite Cement. It was observed that fine OS particles surrounded the regular hexagonal prism CSH grains (Figure 2). Although calcium carbonate and calcium sulfate possess different crystal structures, the exposed crystal planes of carbonate salt containing calcium atoms provide preferential sites for the nucleation of calcium sulfate, which accelerates the growth of CSH crystals. On the other hand, OS particles are not simply mixed into the resultant composites, but some are embedded in CSH crystals. This special multicomponent crystal structure may affect the characteristics and bioproperties of the resulting composites.

During the self-setting process, CSH crystals must first be dissolved into solution; then, all constitutive cations and anions (Ca^{2+} and SO_4^{2-}) recrystallize with water to form CSD. The

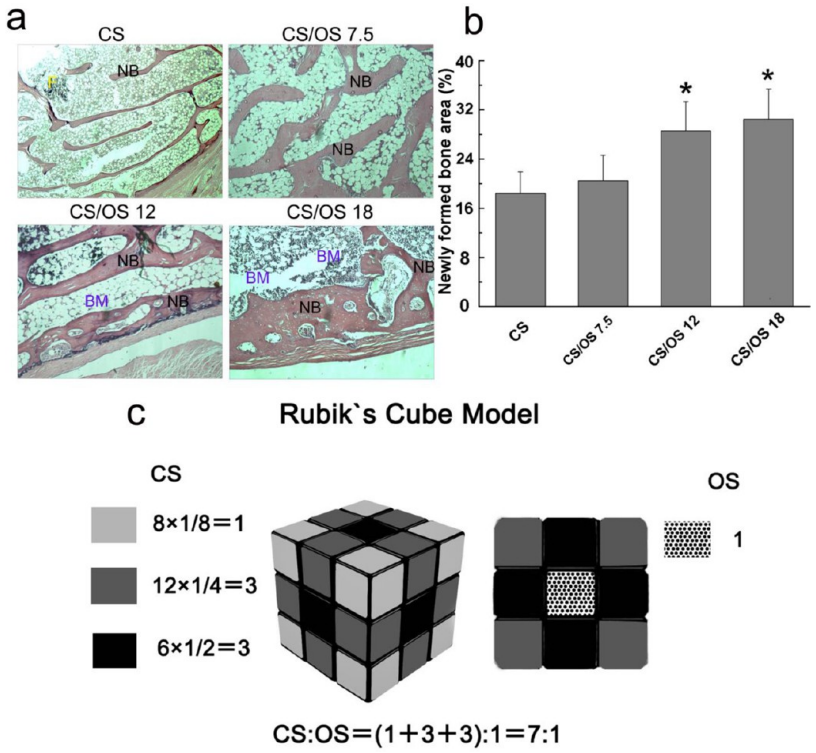

Figure 10. Histological staining with H&E in rabbit femoral defects: (a) Histological observation of new bone formation in rabbit femoral defects model (H&E staining) (F, fibrous tissue; NB, newly formed bone; BM, bone marrow). (b) Quantitative analysis of the new bone area after 8 weeks of surgery by histological observation. * Significant difference between the CS/OS composite pastes and pure CS cement, *$p < 0.05$ (c) Rubik's Cube Model.

hydrogen atoms in a dihydrate crystal strongly interact with oxygen atoms on the surface of surrounding dihydrate crystals; thus, the CSD paste become sticky and acts as a cement. Compared with pure CS cement, the homogeneous CS/OS composite cement showed a delayed setting time (11−28 min), which is attributed to the lack of a hydration reaction for OS (Figure 1b). Analogously, too much sand will make the cement brittle and difficult to coagulate. Similar to sand in a cement, a small amount of OS particles can largely delay the self-setting process. In clinical applications, bone cement must have an appropriate setting time for handling and adjustment during operation. The prolonged setting time of CSH due to the incorporation of OS particles would provide a margin of time for surgeons or dentists to work with the paste during operation.

Moreover, in clinical applications, bone-substitution materials are required to provide adequate mechanical strength to support defect sites. In this study, even though the compressive strength of the CS/OS cements remained low in all cases ($R_{comp} \leq 11$ MPa) (Figure 1), the mechanical strength is sufficiently high for some in vivo applications involving low and even no mechanical stress loading. More specifically, the mechanical strength of the CS/OS composites was maximized with the addition of 12% OS (Figure 1d). To explain this phenomenon, we propose a Rubik's Cube Model (Figure 10c): to achieve good mechanical strength during self-setting, the OS particles must be surrounded completely by CS crystals. After counting the effective number of crystals required, the real OS/CS volume ratio is 1:7, which means that the theoretically ideal OS content is approximately 10 wt %. Our study actually demonstrated that the CS/OS12 composite obtained the highest mechanical strength. The discrepancy between the experimental result and theoretically estimated value can be rationalized by the disparity in the dimensions and shapes of the OS and CS particles. Moreover, the size distribution and aggregation of OS is a decisive factor that determines the required OS content. Consequently, the critical content of OS can exceed 10 wt %. If an excessive amount of OS particles are added to a composite system, CS particles cannot guarantee the full coverage of OS particles, which is why CS/OS25 presented a lower mechanical strength.

4.2. In Vitro Bioactivity and Degradation of the Composite Cement. It is commonly accepted that bone-like hydroxyapatite (HA) plays an important role in maintaining the bone tissue−biomaterial interface.[34] As indicated by multiple studies, pure CS cement always fails to form a chemical bond with bone tissue during the initial stages of therapy due to its poor bioactivity,[10,11,35] which is also confirmed by examination of the surface of pure CS after soaking (Figure 3a and b). However, the combined XRD (Figure 4b), SEM (Figure 3), and EDX analyses (Figure 4a) suggest that the novel CS/OS composite can induce apatite deposition on the surface, demonstrating that the composite exhibits satisfactory bioactivity. Such a result could be attributed to the addition of OS with proven bioactivity. This finding confirms our assumption that the addition of bioactive OS could result in a biomedical composite with improved bioactivity. The chemical reaction associated with this process might be as follows:

$$10CaCO_3 + 6HPO_4^{2-} + 2H_2O \rightarrow Ca_{10}(PO_4)(OH)_2 + 6CO_3^{2-} + 4H_2CO_3$$

This result conforms with the results of Kim's study,[36] which indicate that calcium carbonate has sufficient bioactivity to convert to carbonated hydroxyapatite in SBF. EDS analysis (Figure 4a) further supports that the apatite-like phase is indeed composed of the elements C, O, P, and Ca. The existence of C in apatite crystals, the combination often referred to as carbonated apatite, allows for better biocompatibility and bioresorption rates than those of pure hydroxyapatite[37] due to the material's similarity to the natural mineral component of vertebrates' hard tissue (such as bone and teeth).[38,39] As a natural biomineralized material, OS has the ability to form carbonated apatite, which may enhance CS/OS composites by forming a stronger bond with adjoining bone tissue.

Degradability is another important aspect to consider in evaluating implanted biomaterials, which is determined by the chemical structure and the physical characteristics of materials. One of the main challenges faced by pure CS is the material's rapid rate of degradation, which cannot match the rate of bone regeneration. In our study, the CS/OS composites presented a significantly delayed degradation rate compared to the degradation rate of pure CS (Figure 5c). The delayed degradation rate is attributed to the fact that the additive OS particles exhibit significantly low solubility. Either the embedded OS particles on the surface of CSD crystals or free OS particles among CS particles could retard the penetration of SBF solution and reduce their degree of contact. Moreover, the presence of OS particles could provide a better microenvironment around the implantation location due to the chemical stability and weak ionization of carbonic acid molecules. Moreover, a solution with higher pH might facilitate the acid exudation of pure CS in clinic applications.[30] Duplat et al.[19] observed that the degradation of OS was mainly based on physicochemical factors, whereas living cells mediating in an absorbing manner played limited role on the degradation. Duplat et al.[40] also indicated that the high mineral content of OS and calcium release into resorption lacunae would trigger the inhibition of osteoclast activity.[41,42] Our results also indicate that Ca^{2+} ions are released during soaking in SBF. Maeno et al.[43] concluded that 2−4 mM Ca^{2+} is suitable for the proliferation and survival of osteoblasts, whereas slightly higher concentrations (6−8 mM) favor osteoblast differentiation and matrix mineralization in both two- and three-dimensional cultures. Higher concentrations (410 mM) are cytotoxic. Figure 5a demonstrates that the Ca^{2+} release of the CS/OS composites occurred more smoothly during the degradation period and more closely approached the most suitable Ca^{2+} concentration (6−8 mM) after 1 week. To summarize, the degradation rate and microenvironment of the CS/OS composite pastes was ameliorated by the addition of OS.

4.3. In Vitro Cell Proliferation and Osteogenic Differentiation of the Composite. In vitro cell−material interaction is a standard criterion for evaluating biomaterials. It has been observed that the organic matrix of oyster shells contains diffusible molecules that trigger the differentiation and proliferation of osteoblasts.[27] In our present study, all samples showed no distinct cytotoxicity toward MG-63 cells. Moreover, results suggested that the extraction soluble matrix of the CS/OS composite could provide adequate stimulus for cell proliferation. Combes et al.[44] revealed that the excellent cytocompatibility of calcium carbonate cement is attributed to pH stability during the setting process and the low solubility involved. Another advantage of calcium carbonate cement is that calcium and carbonate ions are noncytotoxic metabolites under the metabolic control of the organism. Furthermore, Berland et al.[32] implanted nacre into sheep bone tissue and revealed that size, shape, and cellular environment are key factors that determine the biodegradation kinetics in a living system. Our present study showed that the CS/OS composites are not only biocompatible and noncytotoxic but also possess excellent bioactivity at the cellular level.

To identify the active molecules in the CS/OS composites and determine their mode of osteogenic action in human osteoblast-like cells, in vitro assays were carried out. Based on ALP and Von Kossa staining, MG-63 cells treated with extracts from the CS/OS composites showed dramatically increased ALP activity and mineralization deposition, where CS/OS18 presented a 2.1-fold increase in mineralized nodule deposition compared with the CS group. Our findings are consistent with those of Lamghari et al.,[22,23] who also observed that OS provided stimulation to osteogenic bone marrow cells with enhanced alkaline phosphatase activity. The authors concluded that OS contains one or more signaling molecules capable of activating osteogenic ability. With respect to molecular events, the CS/OS composites present activating effects for gene markers of osteogenic differentiation: Runx2 and BMP-2 and two late-stage markers, Osterix and OCN. The oyster molecules present in the extraction of CS/OS appear to be responsible for the enhanced osteogenic differentiation by greatly up-regulating Runx2 and BMP-2 expression. Accordingly, the levels of Osterix and OCN gene expression in the CS/OS group were dramatically higher at the 14th day compared with those of the CS group. Interestingly, it appears that the oyster shell particles became involved in osteogenetic activity mainly for osteoblast maturity as osteocytes became mineralized by calcium deposition. Moreover, osteogenic marker proteins, including Col I and BMP-2, were clearly expressed and up-regulated in the CS/OS group, according to Western Blot analysis. This finding also supports that the CS/OS scaffolds were suitable for osteogenic differentiation at the protein level. Zhou's study[45] showed that Pf-Smad3 in oysters is highly similar to the Smad3 proteins in vertebrates and that Pf-Smad3 might take part in many physiological processes such as biomineralization. Osteogenic differentiation is regulated by a wide range of biological molecules interacting together and involved in multiple signaling pathways (such as MAPK, Wnt, and Notch), which form a very complex network of molecular interactions that is not yet fully understood.

4.4. In Vivo Bone Regeneration Ability of the Composite in Rabbit Femoral Defect. Further in vivo studies were performed to confirm the stimulatory osteoanagenesis effect of the CS/OS composites. A rabbit femoral defect model was used to evaluate bone formation ability. Histological observation by HE staining and quantitative analysis was performed after 8 weeks of surgery. The results revealed that administration of the CS/OS composites increased the rate of bone mineralization, bone thickness, and the amount of mineralized bone matrix. The novel CS/OS composites showed suitable performance in promoting new bone formation in rabbit femoral defect repair. In contrast, many previous investigations have reported that calcium sulfate as a bone graft substitute is rapidly resorbed in vivo, releasing calcium ions, but fails to provide a long-term three-dimensional framework to support osteoconduction.[11] Although not fully understood, our in vivo results suggest that CS/OS biomaterials could be gradually replaced by newly formed bone tissue and present satisfactory osteoinduction and osteoconduction. Based

on the results of our study, considering the requirements of sufficient mechanical strength, appropriate setting properties and satisfactory bioactivity both in vitro and in vivo, we recommend the CS/OS12 composite as the optimum composition ratio.

Overall, the novel biomaterial synthesized in this study using calcium sulfate and oyster shell has the potential to be further applied as a feasible and biocompatible substitute for the clinical treatment of bone defects.

5. CONCLUSION

This study represents the first time that natural biomineralized oyster shell has been combined with artificially synthesized calcium sulfate material to create a novel bioactive composite. CS/OS composite cement with a delayed setting time (11−28 min) and high mechanical strength can produce bone-like apatite in SBF solution. The composite cements synthesized in this study can stimulate cell proliferation. Furthermore, the CS/OS composite cements showed slower degradation rates in vitro. Importantly, in the CS/OS composites, increased mineral nodule formation, ALP activity, and elevated mRNA levels of key osteogenic genes, including BMP-2, Runx2, Osx, and OCN, were observed. In vivo, the CS/OS scaffolds strongly promoted osteogenic tissue regeneration in a rabbit femur cavity defect model, as indicated by the results of histological staining. In summary, the present study demonstrates a viable method for designing self-setting biomaterials with improved properties that exploit the advantages of conventional self-setting calcium sulfate hemihydrate and natural bioactive oyster shell. The resultant composite biomaterials are very promising candidates for facilitating osteoanagenesis in clinic treatment.

■ ASSOCIATED CONTENT

Ⓢ Supporting Information

Morphology of specimens before SBF soaking and SEM images of the surface to CS/OS 18 composite after soaking in SBF and cell proliferation assay of CS/OS7.5 and CS/OS18. This material is available free of charge via the Internet at http://pubs.acs.org/.

■ AUTHOR INFORMATION

Corresponding Authors

*Email: yansurgeon@163.com.
*Email: huangqingphd@163.com.
*Email: penglei7518@163.com.

Author Contributions

#Y.S. and S.Y. contributed equally. The manuscript was written through contributions of all authors. All authors have given approval to the final version of the manuscript.

Notes

The authors declare no competing financial interest.

■ ACKNOWLEDGMENTS

This work was financially supported by National Natural Science Foundation of China (31060135, 81371954); The key project of Zhejiang Provincial Department of science and technology (2011C13033); The Fund of health department of Zhejiang province (2012RCA032).

■ REFERENCES

(1) Burg, K. J.; Porter, S.; Kellam, J. F. Biomaterial Developments for Bone Tissue Engineering. *Biomaterials* **2000**, *21*, 2347−2359.

(2) Younger, E. M.; Chapman, M. W. Morbidity at Bone Graft Donor Sites. *J. Orthop. Traumatol.* **1989**, *3*, 192−195.

(3) Summers, B. N.; Eisenstein, S. M. Donor Site Pain from the Ilium—A Complication of Lumbar Spine Fusion. *J. Bone Jt. Surg., Br. Vol.* **1989**, *71*, 677−680.

(4) Enneking, W. F.; Eady, J. L.; Burchardt, H. Autogenous Cortical Bone Grafts in the Reconstruction of Segmental Skeletal Defects. *J. Bone Jt. Surg., Am. Vol.* **1980**, *62*, 1039−1058.

(5) Gepstein, R.; Weiss, R. E.; Saba, K.; Hallel, T. Bridging Large Defects in Bone by Demineralized Bone-Matrix in the Form of a Powder—A Radiographic, Histological, and Radioisotope-Uptake Study in Rats. *J. Bone Jt. Surg., Am. Vol.* **1987**, *69A*, 984−992.

(6) Tiedeman, J. J.; Garvin, K. L.; Kile, T. A.; Connolly, J. F. The Role of a Composite, Demineralized Bone Matrix and Bone Marrow in the Treatment of Osseous Defects. *Orthopedics* **1995**, *18*, 1153−1158.

(7) Coetzee, A. S. Regeneration of Bone in the Presence of Calcium Sulfate. *Arch. Otolaryngol.* **1980**, *106*, 405−409.

(8) Cui, X.; Zhang, B.; Wang, Y.; Gao, Y. Effects of Chitosan-Coated Pressed Calcium Sulfate Pellet Combined with Recombinant Human Bone Morphogenetic Protein 2 on Restoration of Segmental Bone Defect. *J. Craniofac. Surg.* **2008**, *19*, 459−465.

(9) Thomas, M. V.; Puleo, D. A. Calcium Sulfate: Properties and Clinical Applications. *J. Biomed. Mater. Res., Part B* **2009**, *88B*, 597−610.

(10) Cabanas, M. V.; Rodriguez-Lorenzo, L. M.; Vallet-Regi, M. Setting Behavior and In Vitro Bioactivity of Hydroxyapatite/Calcium Sulfate Cements. *Chem. Mater.* **2002**, *14*, 3550−3555.

(11) Stubbs, D.; Deakin, M.; Chapman-Sheath, P.; Bruce, W.; Debes, J.; Gillies, R. M.; Walsh, W. R. In Vivo Evaluation of Resorbable Bone Graft Substitutes in a Rabbit Tibial Defect Model. *Biomaterials* **2004**, *25*, 5037−5044.

(12) Orsini, G.; Ricci, J.; Scarano, A.; Pecora, G.; Petrone, G.; Iezzi, G.; Piattelli, A. Bone-Defect Healing with Calcium-Sulfate Particles and Cement: An Experimental Study in Rabbit. *J. Biomed. Mater. Res., Part B* **2004**, *68*, 199−208.

(13) Lei, D.; Wardlaw, D.; Hukins, D. W. L. Mechanical Properties of Calcium Sulphate/Hydroxyapatite Cement. *Bio-Med. Mater. Eng.* **2006**, *16*, 423−428.

(14) Gao, C. J.; Gao, J. P.; You, X. D.; Huo, S. J.; Li, X. L.; Zhang, Y.; Zhan, W. H. Fabrication of Calcium Sulfate/Plla Composite for Bone Repair. *J. Biomed. Mater. Res., Part A* **2005**, *73A*, 244−253.

(15) Mamidwar, S.; Weiner, M.; Alexander, H.; Ricci, J. In Vivo Bone Response to Calcium Sulfate/Poly L-Lactic Acid Composite. *Implant Dent.* **2008**, *17*, 208−212.

(16) Mamidwar, S. S.; Arena, C.; Kelly, S.; Alexander, H.; Ricci, J. In Vitro Characterization of a Calcium Sulfate/Plla Composite for Use as a Bone Graft Material. *J. Biomed. Mater. Res., Part B* **2007**, *81B*, 57−65.

(17) Balmain, J.; Hannoyer, B.; Lopez, E. Fourier Transform Infrared Spectroscopy (FTIR) and X-Ray Diffraction Analyses of Mineral and Organic Matrix During Heating of Mother of Pearl (Nacre) from the Shell of the Mollusc *Pinctada maxima*. *J. Biomed. Mater. Res.* **1999**, *48*, 749−754.

(18) Mount, A. S.; Wheeler, A. P.; Paradkar, R. P.; Snider, D. Hemocyte-Mediated Shell Mineralization in the Eastern Oyster. *Science* **2004**, *304*, 297−300.

(19) Duplat, D.; Chabadel, A.; Gallet, M.; Berland, S.; Bedouet, L.; Rousseau, M.; Kamel, S.; Milet, C.; Jurdic, P.; Brazier, M.; Lopez, E. The In Vitro Osteoclastic Degradation of Nacre. *Biomaterials* **2007**, *28*, 2155−2162.

(20) Lee, J. S.; Lee, J. M.; Im, G. I. Electroporation-Mediated Transfer of Runx2 and Osterix Genes to Enhance Osteogenesis of Adipose Stem Cells. *Biomaterials* **2011**, *32*, 760−768.

(21) Bais, M. V.; Wigner, N.; Young, M.; Toholka, R.; Graves, D. T.; Morgan, E. F.; Gerstenfeld, L. C.; Einhorn, T. A. Bmp2 Is Essential for Post Natal Osteogenesis but Not for Recruitment of Osteogenic Stem Cells. *Bone* **2009**, *45*, 254−266.

(22) Lamghari, M.; Almeida, M. J.; Berland, S.; Huet, H.; Laurent, A.; Milet, C.; Lopez, E. Stimulation of Bone Marrow Cells and Bone

Formation by Nacre: In Vivo and In Vitro Studies. *Bone* **1999**, *25*, 91S−94S.
(23) Lamghari, M.; Berland, S.; Laurent, A.; Huet, H.; Lopez, E. Bone Reactions to Nacre Injected Percutaneously into the Vertebrae of Sheep. *Biomaterials* **2001**, *22*, 555−562.
(24) Liao, H.; Mutvei, H.; Hammarstrom, L.; Wurtz, T.; Li, J. Tissue Responses to Nacreous Implants in Rat Femur: An in Situ Hybridization and Histochemical Study. *Biomaterials* **2002**, *23*, 2693−2701.
(25) Rousseau, M.; Pereira-Mouries, L.; Almeida, M. J.; Milet, C.; Lopez, E. The Water-Soluble Matrix Fraction from the Nacre of *Pinctada maxima* Produces Earlier Mineralization of Mc3t3-E1Mouse Pre-Osteoblasts. *Comp. Biochem. Physiol., Part B: Biochem. Mol. Biol.* **2003**, *135*, 1−7.
(26) Shen, Y.; Zhu, J.; Zhang, H.; Zhao, F. In Vitro Osteogenetic Activity of Pearl. *Biomaterials* **2006**, *27*, 281−287.
(27) Mouries, L. P.; Almeida, M. J.; Milet, C.; Berland, S.; Lopez, E. Bioactivity of Nacre Water-Soluble Organic Matrix from the Bivalve Mollusk *Pinctada maxima* in Three Mammalian Cell Types: Fibroblasts, Bone Marrow Stromal Cells, and Osteoblasts. *Comp. Biochem. Physiol., Part B: Biochem. Mol. Biol.* **2002**, *132*, 217−229.
(28) Pan, Z. Y.; Yang, G. Y.; Lou, Y.; Xue, E. X.; Xu, H. Z.; Miao, X. G.; Liu, J. L.; Hu, C. F.; Huang, Q. Morphology Control and Self-Setting Modification of α-Calcium Sulfate Hemihydrate Bone Cement by Addition of Ethanol. *Int. J. Appl. Ceram. Technol.* **2013**, *10*, E219−E225.
(29) Kokubo, T.; Takadama, H. How Useful Is SBF in Predicting In Vivo Bone Bioactivity? *Biomaterials* **2006**, *27*, 2907−2915.
(30) Fernandez, E.; Vlad, M. D.; Gel, M. M.; Lopez, J.; Torres, R.; Cauich, J. V.; Bohner, M. Modulation of Porosity in Apatitic Cements by the Use of α-Tricalcium Phosphate−Calcium Sulphate Dihydrate Mixtures. *Biomaterials* **2005**, *26*, 3395−3404.
(31) Knese, K. H. Bone Formation and Development of Osseous Structure. *Verh. Dtsch. Ges. Pathol.* **1963**, *47*, 35−54.
(32) Berland, S.; Delattre, O.; Borzeix, S.; Catonne, Y.; Lopez, E. Nacre/Bone Interface Changes in Durable Nacre Endosseous Implants in Sheep. *Biomaterials* **2005**, *26*, 2767−2773.
(33) Almeida, M. J.; Pereira, L.; Milet, C.; Haigle, J.; Barbosa, M.; Lopez, E. Comparative Effects of Nacre Water-Soluble Matrix and Dexamethasone on the Alkaline Phosphatase Activity of Mrc-5 Fibroblasts. *J. Biomed. Mater. Res.* **2001**, *57*, 306−312.
(34) Greenspan, D. C.; Zhong, J. P.; LaTorre, G. P. Effect of Surface Area to Volume Ratio on in Vitro Surface Reactions of Bioactive Glass Particulates. *Bioceramics* **1994**, *7*, 55−60.
(35) Jamali, A.; Hilpert, A.; Debes, J.; Afshar, P.; Rahban, S.; Holmes, R. Hydroxyapatite/Calcium Carbonate (Ha/Cc) vs Plaster of Paris: A Histomorphometric and Radiographic Study in a Rabbit Tibial Defect Model. *Calcif. Tissue Int.* **2002**, *71*, 172−178.
(36) Kim, S.; Park, C. B. Mussel-Inspired Transformation of Caco3 to Bone Minerals. *Biomaterials* **2010**, *31*, 6628−6634.
(37) Suchanek, W. L.; Shuk, P.; Byrappa, K.; Riman, R. E.; TenHuisen, K. S.; Janas, V. F. Mechanochemical-Hydrothermal Synthesis of Carbonated Apatite Powders at Room Temperature. *Biomaterials* **2002**, *23*, 699−710.
(38) Donners, J. J. J. M.; Nolte, R. J. M.; Sommerdijk, N. A. J. M. Dendrimer-Based Hydroxyapatite Composites with Remarkable Materials Properties. *Adv. Mater.* **2003**, *15*, 313−316.
(39) Shi, J.; Alves, N. M.; Mano, J. F. Thermally Responsive Biomineralization on Biodegradable Substrates. *Adv. Funct. Mater.* **2007**, *17*, 3312−3318.
(40) Duplat, D.; Gallet, M.; Berland, S.; Marie, A.; Dubost, L.; Rousseau, M.; Kamel, S.; Milet, C.; Brazier, M.; Lopez, E.; Bedouet, L. The Effect of Molecules in Mother-of-Pearl on the Decrease in Bone Resorption through the Inhibition of Osteoclast Cathepsin K. *Biomaterials* **2007**, *28*, 4769−4778.
(41) Lorget, F.; Kamel, S.; Mentaverri, R.; Wattel, A.; Naassila, M.; Maamer, M.; Brazier, M. High Extracellular Calcium Concentrations Directly Stimulate Osteoclast Apoptosis. *Biochem. Biophys. Res. Commun.* **2000**, *268*, 899−903.
(42) Miyauchi, A.; Hruska, K. A.; Greenfield, E. M.; Duncan, R.; Alvarez, J.; Barattolo, R.; Colucci, S.; Zamboninzallone, A.; Teitelbaum, S. L.; Teti, A. Osteoclast Cytosolic Calcium, Regulated by Voltage-Gated Calcium Channels and Extracellular Calcium, Controls Podosome Assembly and Bone-Resorption. *J. Cell Biol.* **1990**, *111*, 2543−2552.
(43) Maeno, S.; Niki, Y.; Matsumoto, H.; Morioka, H.; Yatabe, T.; Funayama, A.; Toyama, Y.; Taguchi, T.; Tanaka, J. The Effect of Calcium Ion Concentration on Osteoblast Viability, Proliferation, and Differentiation in Monolayer and 3D Culture. *Biomaterials* **2005**, *26*, 4847−4855.
(44) Combes, C.; Miao, B.; Bareille, R.; Rey, C. Preparation, Physical-Chemical Characterisation, and Cytocompatibility of Calcium Carbonate Cements. *Biomaterials* **2006**, *27*, 1945−1954.
(45) Zhou, Y.; He, Z.; Li, Q.; Xie, L.; Zhang, R. Cloning and Expression Pattern of a Smad3 Homolog from the Pearl Oyster, *Pinctada fucata*. *Acta Biochim. Biophys. Sin.* **2008**, *40*, 244−252.